


RESEARCH ARTICLE

Biofusion design and parameter optimization for a novel passive assisted knee exoskeleton robot based on eight-bar mechanism

Jun Wei^{1,2,3} , Shizhao Zhang^{1,2,3} and Jianjun Zhang^{1,2,3}

¹School of Mechanical Engineering, Hebei University of Technology, Tianjin, 300401, China

²Hebei Key Laboratory of Robot Perception and Human-Machine Integration, Tianjin, 300401, China

³Intelligent Rehabilitation Device and Detection Technology Engineering Research Center of the Ministry of Education, Tianjin, 300130, China

Corresponding authors: Jun Wei; Email: jun.wei@hebut.edu.cn; Jianjun Zhang; Email: zhjjun@hebut.edu.cn

Received: 18 December 2023; **Revised:** 26 February 2024; **Accepted:** 4 April 2024; **First published online:** 9 May 2024

Keywords: passive assisted exoskeleton robot; knee joint; human–machine interaction; OpenSim simulation

Abstract

In an effort to alleviate the issue of knee joint fatigue and injury during lower limb ambulation, a novel passive assisted exoskeleton robot with human–machine interaction is investigated to assist the movement of the human knee joint. The design of the exoskeleton configuration takes into consideration the physiological structure and gait function of the knee joint, ensuring that it satisfies the requirements for motion, force, and gait function of the knee joint. To explore the interaction between the wearer and the exoskeleton, a human–machine kinematic model after wearing exoskeleton is established, which is instrumental in analyzing the integration motion of the wearer and exoskeleton. In addition, the dynamic and static models of the knee joint after wearing the exoskeleton are established, utilizing the Newton–Euler method and force polygon method, respectively, to evaluate the effectiveness of the exoskeleton. Moreover, the size parameters and spring stiffness of the exoskeleton are optimized, using both human body kinematic model and mechanic model. Furthermore, the effectiveness of the exoskeleton in providing assistance is evaluated through human body simulation, using OpenSim. The results indicate that the exoskeleton significantly reduces the knee joint torque by 48.42%.

1. Introduction

The knee joint serves as a primary hinge for both lower limb motion and walking. However, the joint and surrounding muscles are subjected to prolonged periods of excessive forces during walking, rendering them susceptible to fatigue and injury [1]. As a wearable technology, exoskeletons have the potential to assist human movements and decrease joint damage [2]. Within this field, passive exoskeletons have garnered attention due to their uncomplicated design and self-sufficient energy [3–5]. Hence, the development of a passive exoskeleton capable of supporting the knee joint during exercise is imperative to mitigate knee joint fatigue and injury [6].

Currently, passive exoskeleton [7] that provides support to the knee joint collects dispersed energy during the movement and releases energy [8] to assist when needed. Though beneficial for the knee joint, this approach fails to account for the kinematic and dynamic properties of the knee joint, leading to poor comfort and inadequate after exoskeleton wear. Notably, the center of rotation of the knee joint changes continuously during movement, and its sagittal plane trajectory forms a "J" -shaped straight line [9]. To account for the kinematic characteristics of instantaneous center of the knee joint during human–machine interaction [10, 11], Wang [12] and Yang [13] realized the change of instantaneous center in the process of movement by rotating the mechanism along a specific contour line. In addition, the characteristics of the instantaneous center of the linkage mechanism are used to fit the instantaneous

center trajectory of the knee joint, such as the four-bar mechanism [14], the cross four-bar mechanism [15, 16], and the evolutionary mechanism based on the four-bar mechanism [17].

Lee et al. [17] revealed that the relationship between human joint stiffness, that is, the relationship between joint angle and joint torque, is dynamic in joint motion and reflects the resistance of joints to ground reaction force. To address the dynamic characteristics of knee joint variable stiffness [18], Wang et al. [19] [20] realized the exoskeleton joint stiffness adjustment using spring superposition and mechanical structure locking. Yuan et al. [21] realized the nonlinear change of joint stiffness by changing the spring deformation at different times, enabling effective assistance during stair climbing.

The main contribution of this paper is the design of a novel passive assisted exoskeleton with human–machine interaction to assist the movement of the human knee joint and the optimization of size parameters and spring stiffness of the exoskeleton in terms of the human–machine kinematic model and human mechanic model to achieve optimal movement and assist performance. This paper is arranged as follows. Section 2 presents the design of the biological fusion exoskeleton. Human–machine motion modeling and the dislocation of human–machine binding are described in Section 3. Section 4 establishes the human–machine dynamic model and analyzes changes in human joint torque and internal pressure. In Section 5, the size parameters and spring stiffness of the exoskeleton are refined and optimized, followed by simulation of the human body model after exoskeleton wear to demonstrate its assistive performance. The conclusions are shown in Section 6.

2. Biofusion design of knee exoskeleton

2.1. Mapping of knee joint and exoskeleton

The knee joint is not only a very special way of movement, but also its joint force is variable stiffness. During the movement, the knee joint will change the joint stiffness of the knee joint through the interaction of muscles, connective tissue, and bones, so as to meet the needs of the knee joint stiffness of the human lower limbs in different motion states [22, 23].

In the process of walking, according to the function of the lower limb contact with the ground, a gait cycle is divided into eight stages, which are initial landing (IC), load-bearing reaction period (LR), middle support period (MSt), end support period (TSt), early swing period (PSw), early swing period (ISw), middle swing period (MSw), and end swing period (TSw). During the load-bearing reaction period and the middle of the support phase in a gait cycle, in order to alleviate the impact force of the lower limb landing, the knee joint will have a process of first flexion and then extension. In this process, the knee joint produces a large joint torque to maintain the stability of the knee joint at this time, and the internal pressure of the knee joint also reaches a peak during this stage. Joint angle change, joint torque change, and intra-articular pressure change of the knee joint in a gait cycle are shown in Fig. 1 (a), (b), and (c), respectively.

In the realm of wearable robotics, the exoskeleton is conceptualized as a unified system shared between the human body and exoskeleton itself. Within this system, the human serves as a cognitive decision-maker and motion planner, while the exoskeleton serves to assist, compensate, or replace human motion. In relation to the knee joint's particular traits, the exoskeleton must first possess the ability to respond passively to transition while adapting to the knee joint's movements, thus mitigating and obstructions present during lower limb movement. Secondly, the exoskeleton must exhibit the same variable stiffness characteristics as the knee joint; in doing so, the stiffness changes of the knee joint can be more efficiently matched, ultimately creating optimal assistance. Lastly, the exoskeleton must possess the ability to switch the assist torque, catering to distinct requirements of varied gait moments.

2.2. The configuration of knee joint assisted exoskeleton

To fulfill the design [24] demands originating from the physiological attributes of the knee joint, a novel passive assisted exoskeleton is proposed to assist the human–machine interaction of the knee joint.

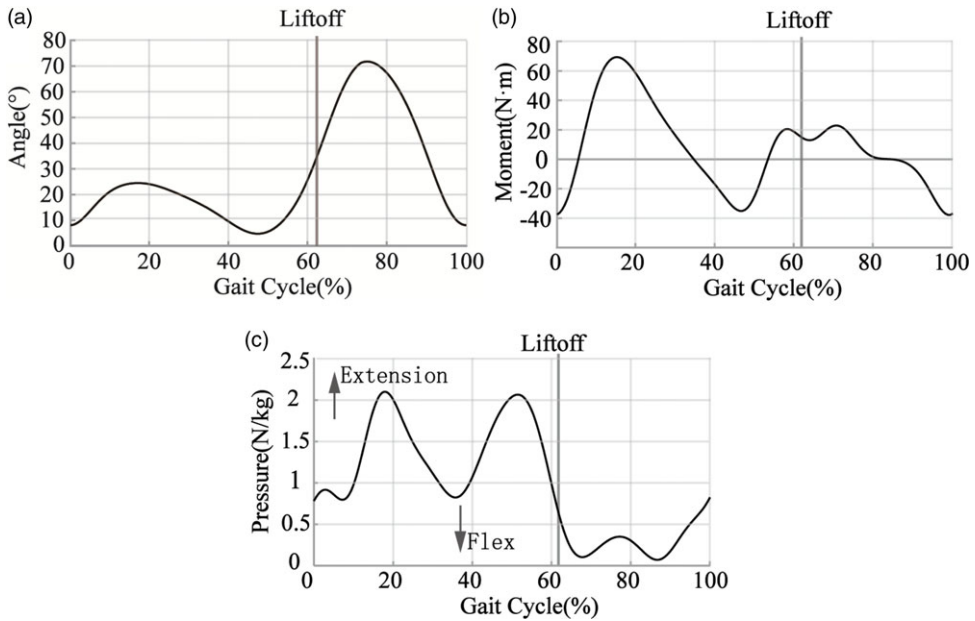


Figure 1. Knee joint movement and force. (a) Changes of knee joint angle during gait cycle. (b) Changes of knee joint torque during gait cycle. (c) Intra-articular pressure changes of knee joint during gait cycle.

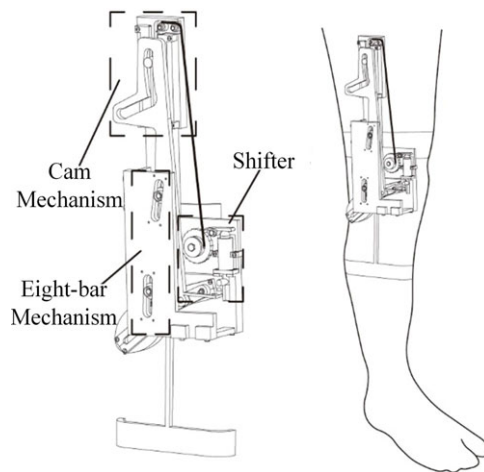


Figure 2. Exoskeleton structure diagram and wearing diagram.

The exoskeleton comprises three primary components, including an eight-bar mechanism, a cam mechanism, and a switching device. The exoskeleton diagram and wearing diagram are shown in Fig. 2, while the structure diagram of the exoskeleton is depicted in Fig. 3.

The eight-bar mechanism is composed of slider components A, B, C, D and rod components AB, CD, EF, which is mainly responsible for the drive of the passive instantaneous center of the exoskeleton. In this mechanism, the rod EF is bound to the human calf and is connected to the rod CD and the rod AB through the revolute pairs E and F, respectively. The instantaneous center points of rod AB and rod CD are located at point M and point N, respectively. The instantaneous center P of rod EF is the intersection of instantaneous center lines NE and MF. The exoskeleton has a single degree of freedom, which meets the motion requirements of the human knee joint.

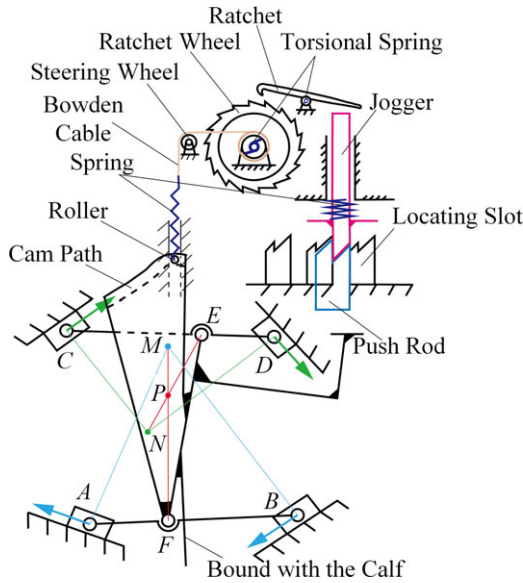


Figure 3. Brief diagram of exoskeleton mechanism.

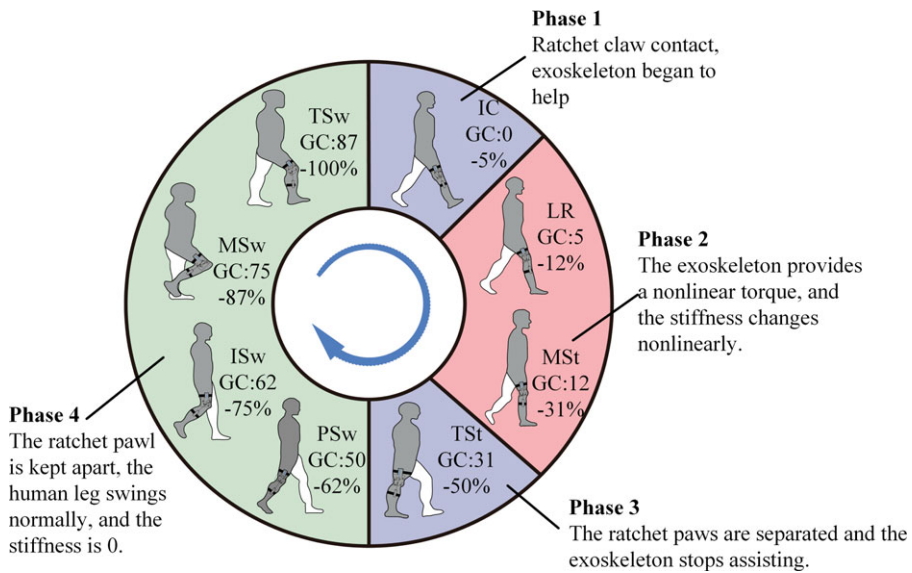


Figure 4. Changes of exoskeleton joint stiffness during gait cycle.

The cam mechanism is mainly composed of a cam and a roller, which mainly realizes the passive variable stiffness of the exoskeleton. The switching device includes a catapult rod, a push rod, a limit rod, a ratchet, a pawl, a Bowden line, and a steering wheel, which realizes the switching of the assist moment and meets the movement needs of the human body at different gait moments.

The switching device employs the number of knee extensions as the switching condition in order to regulate the exoskeleton's assistance phase. This ensures that the exoskeleton provides support during the support phase without interfering with the movement of the knee joint in the swing phase. The workflow of the exoskeleton across the gait cycle (GC) is illustrated in Fig. 4, which is primarily divided into four stages:

1. Knee extension, leg ready to touch the ground (GC: 0–5%). The exoskeleton middle rod EF collides with the push rod, and the ejector rod moves up to make the ratchet pawl in the exoskeleton contact, preparing for the cam pull-down spring when the knee joint is bent and the exoskeleton assists.
2. Knee flexion, human leg to resist the impact of the ground (GC: 5–31%). The cam begins to pull down the spring, and the exoskeleton provides a nonlinear torque to assist. At this time, the exoskeleton joint presents a certain nonlinear stiffness change.
3. Knee extension, human legs support the upper body (GC: 31–50%). The rod EF collides with the push rod again, and the push rod moves down to separate the ratchet and pawl in the exoskeleton. When the knee joint bends again, the exoskeleton will no longer assist, thus not affecting the normal swing of the human leg.
4. Knee flexion, foot off the ground (GC: 50–100%). The cam movement will no longer deform the spring, and the exoskeleton joint stiffness is 0. When the swing phase ends, the knee joint is straightened again and enters the next cycle.

2.3. The working principle of exoskeleton

The rod EF of the eight-bar mechanism is bound with the human calf. As the shank drives the movement of the rod EF, it, in turn, propels the movement of the rods AB and CD. By manipulating the position of the instantaneous center points M and N, the location of the instantaneous center lines NE and MF shifts accordingly, subsequently altering the instantaneous rotation center point P of the exoskeleton.

The cam mechanism realizes the nonlinear change of exoskeleton joint stiffness during the support phase. As the leg rotates, the cam connected with the rod EF follows its downward movement. At this time, the cam will drive the spring to stretch through the pull-down roller. By designing the contour of the cam, the deformation Δx of the spring varies nonlinearly. The joint torque of the exoskeleton is calculated as follows:

$$M = F_T \Delta l = (k \Delta x) \Delta l \quad (1)$$

where M is the exoskeleton joint torque, F_T is spring elasticity, Δl is the distance between the elastic force and the center of rotation, k is spring stiffness, and Δx is a spring shape variable.

In accordance with Eq. (1), as the deformation Δx of the spring varies nonlinearly, the joint torque M of the exoskeleton will also change nonlinearly. As a result, the stiffness of the exoskeleton joint undergoes nonlinear changes during the support phase.

The working principle of the exoskeleton is mainly divided into two stages, namely, the energy storage stage and the energy discharge stage. In the energy storage stage, the exoskeleton moves with the knee joint when the knee joint bends. At this time, the cam mechanism in the exoskeleton stretches the spring to generate nonlinear torque to assist the knee joint movement. While assisting the knee joint to resist the buckling effect caused by the ground reaction force, the exoskeleton converts the kinetic energy in this stage into elastic potential energy and stores it. In the energy discharge stage, when the knee joint ends flexion and begins to return to the straight state, the exoskeleton releases the energy just stored to help the knee joint extend, thus helping the knee joint in this stage. The energy storage and discharge stages of the exoskeleton are shown in Fig. 5.

3. Kinematics of knee exoskeleton with human–machine interaction

3.1. Kinematic model of knee exoskeleton

To investigate the consistency of human–machine motion, kinematic modeling of the eight-bar mechanism is carried out to analyze its instantaneous center trajectory, as shown in Fig. 6. The exoskeleton's thigh rod serves as a fixed frame. The coordinate system $O-XY$ is a plane coordinate system established

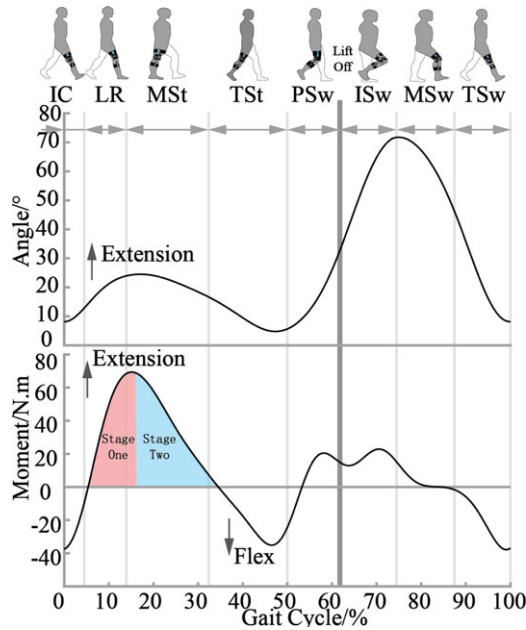


Figure 5. Changes of exoskeleton joint stiffness during gait cycle.

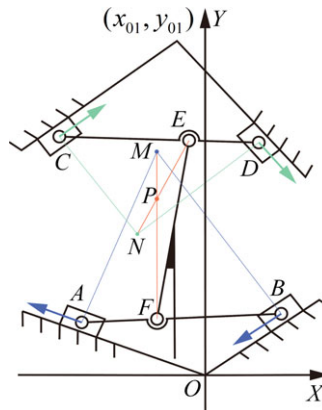


Figure 6. Kinematic analysis of mechanism.

with the intersection of the trajectory extension lines of sliders A and B as the origin O. The trajectory extension lines of sliders C and D intersect at points (x_0, y_0) , whereas the instantaneous center lines of sliders A and B intersect at the point M, and those of sliders C and D intersect at the point N. The instantaneous rotation center of the exoskeleton is the instantaneous center of the rod EF when the exoskeleton is worn. The instantaneous center of the rod EF is the intersection point P of the instantaneous center lines MF and NE, and the coordinate of the instantaneous center point P is (x_p, y_p) . The position of the sliders A, B, C, and D is described by the position of the rotation center of the revolute pair. The positions of the sliders A, B, C, and D are $(x_1, y_1), (x_2, y_2), (x_3, y_3), (x_4, y_4)$, respectively. The distance between the sliders A and B and the coordinate origin is l_1, l_2 , respectively. The distance between the sliders C and D and the point (x_0, y_0) is l_3, l_4 , respectively. Let the angle between the sliders A, B, C, and D and the positive direction of the X axis be $\theta_1, \theta_2, \theta_3, \theta_4$, respectively, and the length of the rod AB, CD, and EF be l_{AB}, l_{CD}, l_{EF} , respectively. The relationship between points E and F on the rods AB

and CD is expressed as $l_{AF} = e_1 l_{FB}$, $l_{CE} = e_2 l_{ED}$, with coordinates for points E and F being (x_5, y_5) and (x_6, y_6) , respectively. The instantaneous center points M and N of the rods AB and CD are described by coordinates (x_7, y_7) and (x_8, y_8) , respectively. When the knee joint is straightened, the angle between the rod EF and the vertical direction is θ_0 . The angle of rotation of the rod EF relative to the vertical direction is θ .

In this coordinate system, the coordinates of sliders A and B are expressed as follows, respectively:

$$\begin{cases} y_i = l_i \cos \theta_i \\ x_i = l_i \sin \theta_i \end{cases} \tag{2}$$

where y_i and x_i represent the coordinates of sliders A and B , l_i represents the distance between sliders A and B and the origin of coordinates, and θ_i represents the positive angle between sliders A and B and X axis, where $i = 1, 2$.

In this coordinate system, the coordinates of the sliders C and D are shown as follows, respectively:

$$\begin{cases} y_j = y_0 + l_j \cos \theta_j \\ x_j = x_0 + l_j \sin \theta_j \end{cases} \tag{3}$$

where y_j and x_j represent the coordinates of C and D , l_j denotes the distance between the C and D distance points (x_0, y_0) of the slider, and θ_j denotes the angle between the sliders C and D and the positive axis, where $j = 3, 4$.

According to the positional relationship $l_{AF} = e_1 l_{FB}$ and $l_{CE} = e_2 l_{ED}$ of points E and F on the rod CD and rod AB , the coordinates of points E and F are obtained as

$$\begin{cases} y_{i1} = \frac{y_{n1} + e_i y_{n2}}{1 + e_i} \\ x_{i1} = \frac{x_{n1} + e_i x_{n2}}{1 + e_i} \end{cases} \tag{4}$$

where y_{i1} and x_{i1} represent the coordinates of points E and F , y_{n1} and x_{n1} represent the table slider A and C coordinates, and y_{n2} and x_{n2} represent the coordinates of sliders B and D , where $i_1 = 5, 6$, $n_1 = 1, 3$, $n_2 = 2, 4$.

According to the angle $\theta + \theta_0$ between the pole EF and the vertical direction, the following relationship between points E and F can be deduced:

$$\begin{cases} x_6 - x_5 = l_{EF} \sin(\theta + \theta_0) \\ y_6 - y_5 = l_{EF} \cos(\theta + \theta_0) \end{cases} \tag{5}$$

where l_{EF} is the length of the rod EF , θ_0 is the angle between the EF and the vertical direction when the leg is straight, and θ is the angle of the rod EF relative to the vertical direction.

According to the relations in Eqs. (3) and (4), the relations between l_3, l_4 and l_1, l_2 are obtained, respectively:

$$\begin{cases} l_3 = \frac{(e_2 + 1) [(e_1 + 1) l_{EF} \cos(\theta + \theta_2) + l_1 \sin(\theta - \theta_2)]}{(e_1 + 1) \sin(\theta_1 - \theta_2)} \\ l_4 = \frac{-(e_2 + 1) [(e_1 + 1) l_{EF} \cos(\theta + \theta_1) + e_1 l_2 \sin(\theta_1 - \theta_2)]}{e_2 (e_1 + 1) \sin(\theta_2 - \theta_1)} \end{cases} \tag{6}$$

Through the instantaneous center line perpendicular to the slider trajectory, the coordinates of the instantaneous center points M and N of the rods AB and CD satisfy the following relationship:

$$\begin{cases} \frac{y_{i2} - y_{n1}}{x_{i2} - x_{n1}} = -\frac{1}{\tan \theta_{n1}} \\ \frac{y_{i2} - y_{n3}}{x_{i2} - x_{n3}} = -\frac{1}{\tan \theta_{n2}} \end{cases} \tag{7}$$

where y_{i2} and x_{i2} represent the coordinates of the instantaneous center points M and N and y_{n3} and x_{n3} represent the coordinates of the recalculated slider C and slider D , where $i_2 = 7, 8; n_3 = 3, 4$.

According to Eq. (8), the coordinates of the instantaneous center points M and N are expressed as

$$\begin{cases} y_{i2} = \frac{x_{n1} - x_{n3} + y_{n1} \cdot \tan \theta_{n1} - y_{n3} \cdot \tan \theta_{n2}}{\tan \theta_{n1} - \tan \theta_{n2}} \\ x_{i2} = \frac{x_{n3} \cdot \tan \theta_{n1} - x_{n1} \cdot \tan \theta_{n2} + (y_{n3} - y_{n1}) \cdot \tan \theta_{n1} \cdot \tan \theta_{n2}}{\tan \theta_{n1} - \tan \theta_{n2}} \end{cases} \quad (8)$$

Assuming that the instantaneous center lines FM and NE pass through the instantaneous rotation center of the knee joint (taking the average $x = 15, y = 117$),

$$\frac{y_{i2} - 117}{x_{i2} - 15} = \frac{y_{i1} - 117}{x_{i1} - 15} \quad (9)$$

According to Eq. (10), the relationship between l_1 and l_2 can be obtained (see in Appendix A):

$$l_1 = \frac{\sqrt{N_{11}l_2^2 + N_{12}l_2 + N_{13}} + N_{21}l_2 + N_{22}}{N_{31}} \quad (10)$$

$$l_2 = \frac{M_{41} - \sqrt{M_{11}l_2^2 + M_{12}l_2 - M_{13}} + M_{12}l_2 + M_{22}}{M_{31}} \quad (11)$$

Based on the relationship between the instantaneous rotation center lines FM and NE and the instantaneous rotation center point P , the relationship between the instantaneous center point P and the instantaneous center points M and N can be obtained:

$$\begin{cases} \frac{y_7 - y_P}{x_7 - x_P} = \frac{y_6 - y_P}{x_6 - x_P} \\ \frac{y_8 - y_P}{x_8 - x_P} = \frac{y_5 - y_P}{x_5 - x_P} \end{cases} \quad (12)$$

where (x_p, y_p) is the coordinate of the instantaneous rotation center P of the exoskeleton.

The coordinates of points M and N are substituted into Eq. (13) to obtain the instantaneous rotation center P of the exoskeleton:

$$\begin{cases} x_P = \frac{y_5y_6(x_8 - x_5 - x_7) + y_7y_8(x_5 - y_5 + x_7 - x_6)}{(y_6 - y_7)^2(y_5 - y_8 - x_5 + x_8)} + \frac{(x_7y_6^2 - y_7y_6x_6)(y_5 - y_8 - x_5 + x_8)}{(y_6 - y_7)^2(y_5 - y_8 - x_5 + x_8)} \\ \quad + \frac{(x_7y_7y_6 - y_7^2x_6)(y_8 - y_5 + x_5 + x_8)}{(y_6 - y_7)^2(y_5 - y_8 - x_5 + x_8)} \\ y_P = \frac{y_5y_6(x_8 - x_5 - x_7) + y_7y_8(x_5 - y_5 + x_7 - x_6)}{(x_6 - x_7)(y_5 - y_8) - (x_5 - x_8)(y_6 - y_7)} \end{cases} \quad (13)$$

3.2. Human-machine coupling kinematic model of knee exoskeleton

To facilitate the analysis of the intricate movement of the lower limbs when wearing the exoskeleton, a simplification is performed whereby the exoskeleton and lower limbs are treated as two separate entities connected by a thigh rod and a calf rod through a specialized motion joint. The thigh portion of the human-machine is fixed in place, while the connection of the calf part is visualized as a PS branch chain. The simplified human-machine lower limb model and the human-machine calf space single closed chain with one degree of freedom are shown in Fig. 7.

The kinematics of the spatial single closed chain comprised of human-machine calf rods is described as follows: The initial position coordinate system of the exoskeleton is denoted as $O_p-x_p y_p z_p$. The initial position coordinate system of human body is represented by $O_o-x_o y_o z_o$. The rotation center coordinate system after the rotation of the calf is labeled by $O_1-x_1 y_1 z_1$. The slider position coordinate system

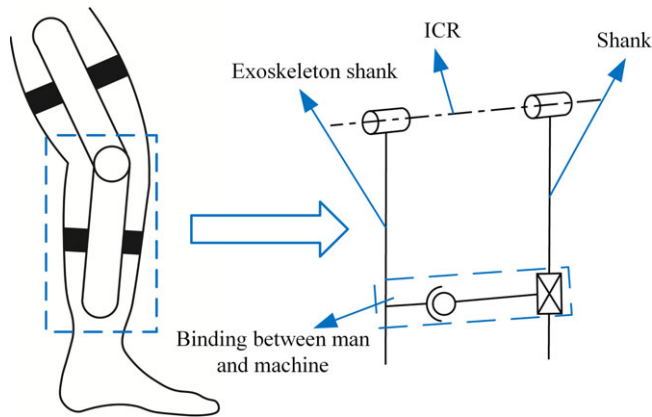


Figure 7. Simplified lower limb model after wearing exoskeleton and single closed chain of human-machine calf space.

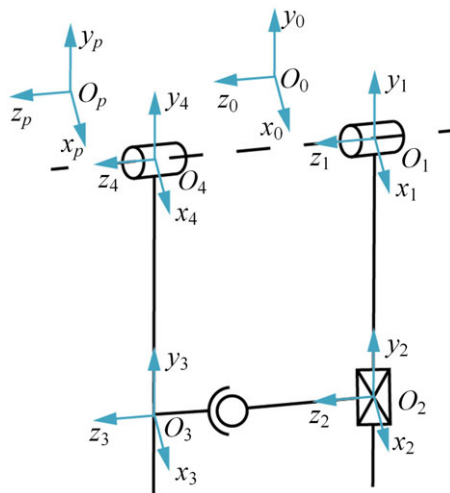


Figure 8. Kinematic description of single closed chain in man-machine calf space.

is designated as $O_2-x_2y_2z_2$, while the coordinate system at the connection between the ball pair and the exoskeleton bar is $O_3-x_3y_3z_3$. Finally, the coordinate system of the rotation center position after the exoskeleton rotates is registered as $O_4-x_4y_4z_4$. The kinematic description of spatial single closed connection is shown in Fig. 8.

After the exoskeleton rotates β degree, the transformation matrix for the coordinate $O_4-x_4y_4z_4$, coupled with the rotation center of the exoskeleton, compared to the coordinate $O_p-x_p y_p z_p$ aligned with the initial point of the exoskeleton, is given as follows:

$$\begin{aligned}
 {}^p_4T &= {}^p_0T_1 T_2^1 T_3^2 T_4^3 T \\
 &= \begin{pmatrix} c\alpha \cdot c\theta - s\alpha \cdot s\theta & -c\alpha \cdot s\theta - s\alpha \cdot c\theta & 0 & -c\alpha \cdot s\theta \cdot l_e - s\alpha \cdot c\theta \cdot l_e + l_m \cdot s\alpha + x_\alpha \\ s\alpha \cdot c\theta + c\alpha \cdot s\theta & -s\alpha \cdot s\theta + c\alpha \cdot c\theta & 0 & -s\alpha \cdot s\theta \cdot l_e + c\alpha \cdot c\theta \cdot l_e - l_m \cdot c\alpha + y_\alpha \\ 0 & 0 & 1 & 0 \\ 0 & 0 & 0 & 1 \end{pmatrix} \quad (14)
 \end{aligned}$$

Table I. Exoskeleton size parameters.

Design variable	Value ranges	Design variable	Value ranges	Design variable	Value ranges
l_{AB}/mm	51.12	$\theta_D/^\circ$	274.97	l_e/mm	140
l_{CD}/mm	76.79	$\theta_0/^\circ$	-14.68		
l_{EF}/mm	20.03	x_{01}/mm	95.53		
$\theta_A/^\circ$	56.52	y_{01}/mm	62.26		
$\theta_B/^\circ$	0.51	e_1	17.16		
$\theta_C/^\circ$	194.97	e_2	1.08		

With the exoskeleton’s rotation by β degree, the rotation angle of the exoskeleton leg with respect to its initial point can be determined by combining it with Eq. (16), resulting in

$$\begin{cases} \cos \beta = \cos \alpha \cos \theta - \sin \alpha \sin \theta \\ \sin \beta = \sin \alpha \cos \theta + \cos \alpha \sin \theta \end{cases} \tag{15}$$

where β is the rotation angle of the exoskeleton calf rod.

According to Eq. (17), the relationship between the rotation angle β of the exoskeleton calf and the rotation angle α of the human calf is

$$\beta = \alpha + \theta \tag{16}$$

When the exoskeleton rotates β , according to the position of the rotation center of the exoskeleton at this time, combined with Eq. (16), it can be seen that

$$\begin{cases} x_\beta = -l_e \sin \beta + l_m \sin \alpha + x_\alpha \\ y_\beta = l_e \cos \beta - l_m \cos \alpha + y_\alpha \end{cases} \tag{17}$$

where (x_β, y_β) is the coordinate of the exoskeleton rotation center when the exoskeleton rotates β .

According to Eq. (17), the distance l_m of the rotation center of the knee joint after the slider rotates α relative to the human knee joint is shown as

$$\begin{cases} l_m = \frac{x_\beta + l_e \sin \beta - x_\alpha}{\sin \alpha} \\ l_m = \frac{-y_\beta + l_e \cos \beta + y_\alpha}{\cos \alpha} \end{cases} \tag{18}$$

The relationship between the exoskeleton rotation angle β and the human knee joint rotation angle α is obtained by eliminating l_m in Eq. (19):

$$x_\beta + l_e \cdot \sin \beta = (-y_\beta + l_e \cdot \cos \beta) \cdot \tan \alpha + y_\alpha \cdot \tan \alpha + x_\alpha \tag{19}$$

Assuming the human knee joint is not rotated, the distance between the exoskeleton and the center of rotation of the knee joint is considered to be the length l_e from the exoskeleton to the center of rotation. Wearing the exoskeleton, the deviation at the leg binding is displaced as

$$z = l_e - l_m \tag{20}$$

where z is the dislocation at the leg binding.

Based on the correlation between the rotation angle β of the exoskeleton and the rotation angle α of the human knee joint, as outlined in Eq. (18), if one of these angles is known, the other can be derived. Utilizing Eqs. (18) and (20), the position deviation and rotation angle between the exoskeleton shank and the human shank can be obtained.

In order to verify the correctness of the man-machine kinematic model, the simulation analysis is carried out. The exoskeleton size parameters are shown in Table I.

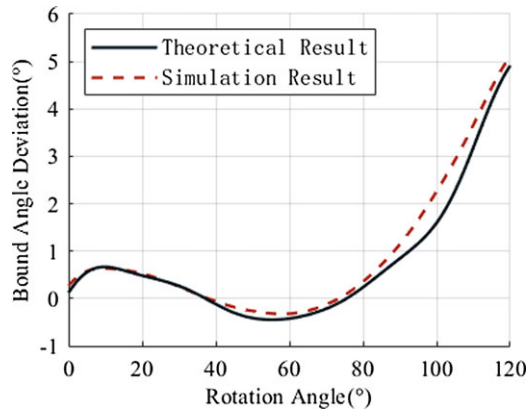


Figure 9. Human-machine instantaneous center trajectory.

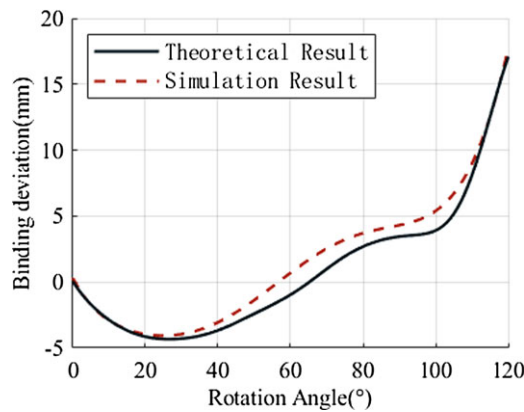


Figure 10. Theoretical results and simulation results of sliding degree.

According to the size parameters in Table I, the instantaneous center trajectory of the exoskeleton under this size is calculated as shown in Fig. 9, and the degree of deviation dislocation at the human-machine binding is obtained by simulation as shown in Fig. 10. The simulation and theoretical results of the degree of rotation dislocation are shown in Fig. 11.

According to Figs. 9 and 10, it can be seen that the simulation of the human-machine kinematic model is basically the same as the theoretical trend. The human-machine kinematic model proposed in this paper can reflect the degree of deviation and rotation at the binding between human and machine to a certain extent.

4. Assist performance of knee exoskeleton

4.1. Dynamic model of knee exoskeleton

During the LR and MSt phases of human gait, the thighs in the lower limbs remain relatively immobile, while the calves revolve around the knee joint in response to the ground reaction force. As a result, the lower limbs, after wearing the exoskeleton, are simplified, where the human-machine thigh components become consolidated, while the human-machine calf components act in concert to counteract the impact force imposed on the ground. The interplay between angle relationship and force relationship of the human-machine lower limb is depicted in Fig. 12.

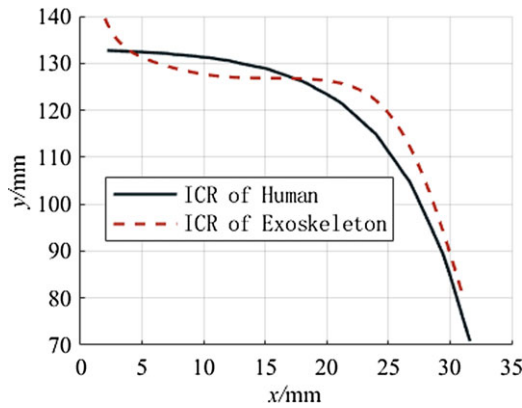


Figure 11. Rotation degree theoretical results and simulation results.

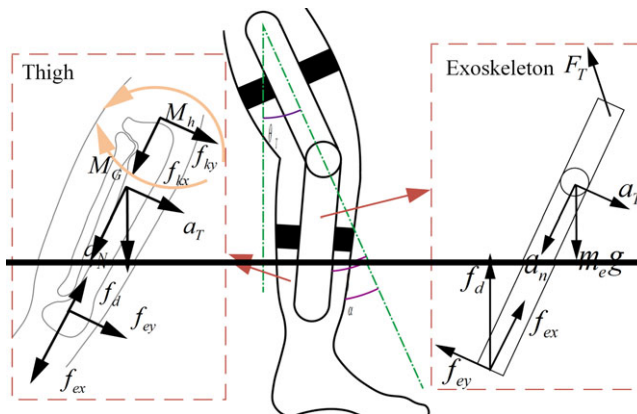


Figure 12. The angle of each part during knee flexion.

The dynamic equation [25] of the exoskeleton calf rod is written by Newton–Euler method:

$$\begin{cases} m_e a_n = -F_T \cos \beta + m_e g \cos(\beta - \theta_i) + f_d \cos \theta - f'_{ex} \\ m_e a_t = -F_T \sin \beta + m_e g \sin(\beta - \theta_i) + f_d \sin \theta - f'_{ey} \\ J_e \ddot{\theta}_e = F_T l_T \sin \beta + m_e g l_{me} \sin(\theta_i - \beta) + f_d l_e \sin \theta - f'_{ey} l_e \end{cases} \quad (21)$$

where m_e is the mass of the exoskeleton shank. F_T is the elastic force generated by the spring in the exoskeleton. θ_i is the angle between the thigh and the vertical direction. f'_{ex} is the projection of the human–computer interaction force in the direction perpendicular to the calf rod during the human–machine interaction process. f'_{ey} is the projection of human–machine interaction force along the direction of the calf rod in the process of human–machine interaction. J_e is the rotational inertia of the exoskeleton calf rod. $\ddot{\theta}_e$ is the angular acceleration of the exoskeleton calf rod. l_T is the projection of the distance from the roller center to the exoskeleton rotation center along the direction of the calf rod. l_{me} is the projection of the distance from the center of mass of the exoskeleton calf rod to the center of rotation of the exoskeleton along the direction of the calf rod.

The motion trajectory of the roller is selected as

$$s = a \sin(b\beta) + c \cos(d\beta) + e \quad (22)$$

where s is the trajectory of the roller and a , b , c , d , and e are parameter variables, respectively.

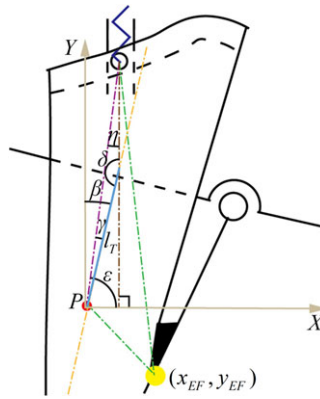


Figure 13. Auxiliary line in exoskeleton.

The spring elastic force generated by the exoskeleton pulling spring is given as

$$F_T = k_0 \cdot \Delta l \tag{23}$$

where k_0 is the stiffness coefficient of the spring and Δl is the compression of the spring, where $\Delta l = s$.

The force produced by the deformation of human leg can be calculated according to the Voith element simulating viscoelasticity:

$$f_d = kd + \dot{d}b \tag{24}$$

where k is the stiffness of human skin, d is the displacement of the binding, \dot{d} for displacement velocity, and b is the friction force at the man-machine binding.

An auxiliary line is established linking the center of the roller in the exoskeleton, the midpoint of the rod EF, and the rotation center of the exoskeleton, as illustrated in Fig. 13.

Based on the geometric relationship illustrated in Fig. 13, the following conditions can be obtained:

$$\varepsilon = \arctan\left(\frac{y_l}{x_l}\right) \tag{25}$$

$$\gamma = \varepsilon - \frac{\pi}{2} + \beta \tag{26}$$

$$\eta = \arctan\left(\frac{x_l}{y_l}\right) \tag{27}$$

$$\delta = \pi - \gamma - \eta \tag{28}$$

According to the sine theorem, the distance from the roller center to the exoskeleton rotation center in the direction of the exoskeleton calf rod is expressed as

$$l_T = \frac{\sin \eta}{\sin \delta} \sqrt{x_l^2 + y_l^2} \tag{29}$$

Assuming that the exoskeleton shank is a homogeneous rod, the length of the rod is shown as follows:

$$l_a = l_e + \cos \gamma \cdot \sqrt{x_l^2 + y_l^2} \tag{30}$$

where l_a is the length of the exoskeleton calf rod.

The distance from the center of mass of the exoskeleton shank to the center of rotation is given as follows:

$$l_{me} = \frac{l_a}{2} - l_e \tag{31}$$

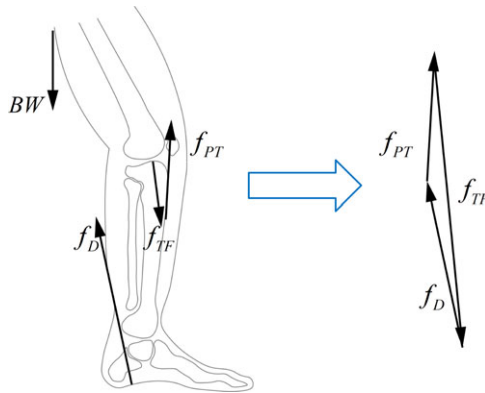


Figure 14. Static model of knee joint.

According to Eqs. (25), (26), (31), and (33), the other unknowns in the exoskeleton dynamic Eq. (23) have been obtained. So far, the human–machine interaction force at the binding can be obtained through Eq. (23).

The dynamic equation of human calf is written by Newton–Euler method:

$$\begin{cases} m_h a_N = m_h g \sin(\alpha - \theta_t) + f_{ey} + f_{ky} \\ m_h a_T = m_h g \cos(\alpha - \theta_t) + f_{ex} + f_{kx} + f_d \\ J_h \ddot{\theta}_h = M_G - M_h - m_h g l_h \sin(\theta_t - \alpha) / 2 - f_{ey} l_m \end{cases} \quad (32)$$

where m_h is the mass of human calf. f_{ex} is the projection of human–machine interaction force perpendicular to the calf direction in the process of human–machine interaction. f_{ey} is the projection of human–machine interaction force along the calf direction in the process of human–machine interaction. J_h is the moment of inertia of the human calf. $\ddot{\theta}_h$ is the angular acceleration of the knee joint. f_{kx} is the force along the x direction at the knee joint. f_{ky} is the force along the y direction at the knee joint. l_h is the leg length. M_G is the ground reaction force to produce knee flexion moment. M_h is the torque of the knee joint to resist the flexion effect generated by the ground reaction force.

4.2. Static model of human body

When the knee joint muscle force resists the flexion effect caused by the ground reaction force, the muscle force drives the femur and tibia closer together, thereby increasing the internal pressure within the joints. To mitigate this effect, the exoskeleton assists the knee joint to resist the ground reaction force by applying human–machine interaction force to the binding site, reducing the muscle force and intra-articular pressure of the knee joint. To analyze the changes in pressure within the knee joint during this process, a static analysis is performed on the knee joint while under a certain instantaneous state, which establishes a relationship between the pressure within the knee joint and the muscle force. The static model of the knee joint is shown in Fig. 14.

According to Eq. (33), the joint torque M_h of the knee joint is calculated. By consulting the relevant medical literature, the force of the quadriceps femoris of the knee joint applied to the tibia to the force arm l_{PT} of the instantaneous rotation center of the knee joint is obtained. According to the torque formula, the force applied to the tibia by the quadriceps of the knee joint is shown as follows:

$$f_{PT} = \frac{M_h}{l_{PT}} \quad (33)$$

where f_{PT} is the force exerted on the tibia by the quadriceps and l_{PT} is the torque applied to the tibia by the quadriceps to the instantaneous rotation center of the knee joint.

Table II. Exoskeleton size parameters and spring stiffness.

Design variable	Value ranges	Design variable	Value ranges
<i>a</i>	−15.153	<i>d</i>	14.056
<i>b</i>	0.016	<i>e</i>	17.418
<i>c</i>	1.042	<i>k</i> ₀ / (N.mm ^{−1})	10

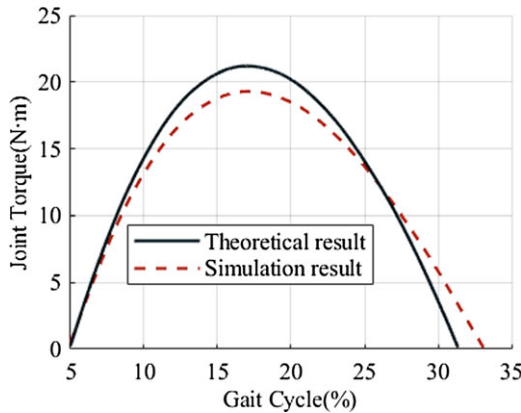


Figure 15. Torque of human knee joint.

During a certain moment in the weight-bearing reaction period, the knee joint maintains the balance for the lower limbs of the human body through the combined influence of ground reaction force, knee joint force, and knee joint pressure. Applying the principles of polygon force distribution, the internal pressure within the knee joint can be obtained as

$$f_{TF} = \sqrt{f_{PT}^2 + f_D^2 - 2f_{PT}f_D \cos(\pi - \alpha - \tau)} \tag{34}$$

where f_{TF} is the force exerted by the femur on the tibia, f_{PT} is the force applied to the tibia by the quadriceps femoris, f_D is the ground reaction force, and τ is the angle between the ground force and the vertical direction.

The angle τ representing the deviation between the ground force and the vertical direction remains relatively stable throughout the entirety of the weight-bearing reaction period, thereby displaying a static discrepancy. When the knee joint angle α undergoes alterations, the internal pressure of the knee joint f_{TF} can be determined based on the internal pressure relationship described in Eq. (34), especially when the knee joint rotates at different angles α .

The exoskeleton size parameters and spring stiffness under the condition of high fitting degree of human joint torque are selected as simulation parameters. The joint torque and intra-articular pressure of knee joint under the action of exoskeleton are simulated and analyzed. The exoskeleton size parameters are shown in Table II.

Under this size parameter and spring stiffness, the fitting degree of the knee joint torque is shown in Fig. 15. The human-machine interaction force is shown in Fig. 16. The theoretical results and simulation results of the joint torque are shown in Fig. 17. The theoretical results and simulation results of the intra-articular pressure are shown in Fig. 18.

Through the simulation analysis of joint torque and intra-articular pressure, it can be seen that the human body mechanic model is basically correct. The human body dynamic model and static model in the human body mechanic model can predict the changes of knee joint torque and intra-articular pressure.

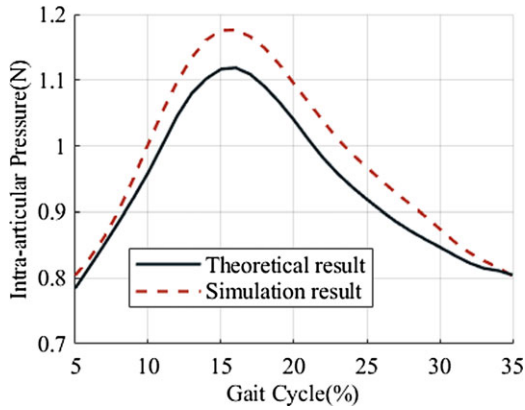


Figure 16. Human-machine interaction force.

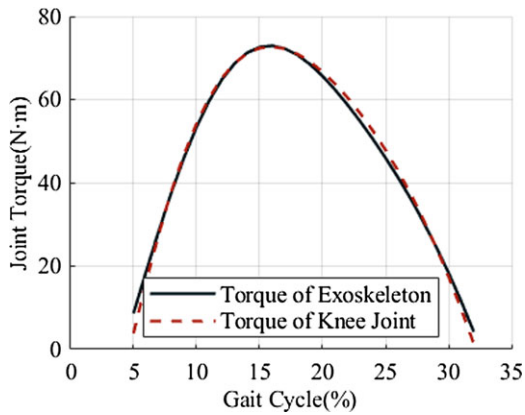


Figure 17. Theoretical results and simulation results of joint torque.

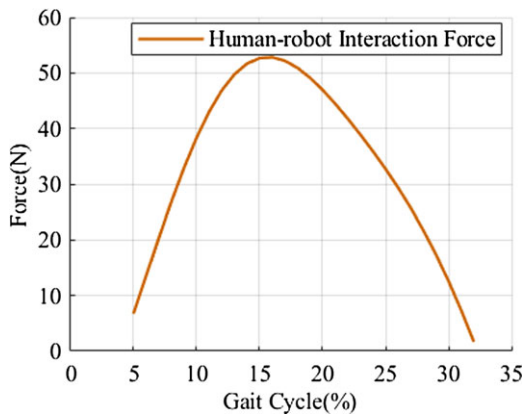


Figure 18. Theoretical and simulation results of knee joint internal pressure.

5. Parameter optimization and simulation analysis of exoskeleton

5.1. Human-machine interaction performance optimization

To achieve greater consistency in human and machine, it is essential to enhance the assist effect of exoskeleton. Drawing upon the human-machine kinematic model and human mechanic model previously developed, a genetic algorithm (GA) is employed to meticulously optimize the size parameters and spring stiffness of the exoskeleton. This optimization endeavor aims to achieve optimal movement and assist performance of exoskeleton when worn by the user.

(1) Design variable

The design variables are independent variables in the optimization process. As described in Eqs. (21), (22), and (33), there are 18 parameters that significantly impact the human-machine kinematic model and dynamic model. Thus, these parameters are selected as the design variables in the exoskeleton optimization model to ensure the optimal performance of the exoskeleton.

$$\begin{aligned} \mathbf{x} &= (x_1, x_2, x_3, x_4, x_5, x_6, x_7, x_8, x_9, x_{10}, x_{11}, x_{12}, x_{13}, x_{14}, x_{15}, x_{16}, x_{17}, x_{18})^T \\ &= (l_{AB}, l_{CD}, l_{EF}, \theta_A, \theta_B, \theta_C, \theta_D, \theta_0, x_{01}, y_{01}, e_1, e_2, a, b, c, d, e, k_0)^T \end{aligned} \tag{35}$$

(2) Objective function

The higher the degree of human-machine interaction after wearing the exoskeleton, the smaller the obstacle to the movement of the calf, thus ensure the comfort and safety of wearing the exoskeleton. Additionally, a smaller joint torque of the knee joint helps to improve the assist performance provided by the exoskeleton to the knee joint. Hence, it is crucial to construct an objective function that reflects the optimization degree of both objectives. This objective function ensures the optimal human-machine interaction motion and exoskeleton assist performance after wearing the exoskeleton.

To minimize the sliding distance and relative rotation angle of the exoskeleton along the lower leg, an objective function that reflects the degree of human-machine interaction motion is established. This objection function utilizes the ideal coordinates of the instantaneous center of the human knee joint every 10° based on the knee flexion angle.

$$S_1 = \sum_{i=1}^{13} \frac{\sqrt{Z^2 + \beta^2}}{2} \tag{36}$$

where S_1 is the objective function of instantaneous center trajectory optimization, Z is the sliding distance of the exoskeleton binding along the leg, and β is the relative rotation angle between human and machine.

To minimize the joint torque and intra-articular pressure of the knee joint simultaneously, an objective function S_2 is established, reflecting the assist performance of the exoskeleton. The torque of the human knee joint is taken every 1% based on the gait cycle

$$S_2 = \sum_{i=1}^{11} \frac{\sqrt{M_h^2 + f_{PT}^2}}{2} \tag{37}$$

where S_2 is the objective function of joint stiffness optimization, M_h is the knee joint torque, and f_{PT} is the pressure in the knee joint.

Using the objective functions S_1 and S_2 , an overall objective function S is constructed that can reflect the fitting degree of the two objective functions:

$$S = \sqrt{\left(\frac{S_1}{13}\right)^2 + \left(\frac{S_2}{11}\right)^2} \tag{38}$$

where S is the objective function that reflects the degree of human-machine coupling motion and exoskeleton assist performance.

Table III. Constraint conditions of exoskeleton parameters.

Design variable	Value ranges	Design variable	Value ranges	Design variable	Value ranges
l_{AB}/mm	20 ~ 90	$\theta_D/^\circ$	180 ~ 360	a	-100 ~ 100
l_{CD}/mm	20 ~ 90	$\theta_0/^\circ$	-60 ~ 60	b	-100 ~ 100
l_{EF}/mm	20 ~ 90	x_{01}/mm	-300 ~ 300	c	-100 ~ 100
$\theta_A/^\circ$	0 ~ 180	y_{01}/mm	-300 ~ 300	d	-100 ~ 100
$\theta_B/^\circ$	0 ~ 180	e_1	1 ~ 20	e	-100 ~ 100
$\theta_C/^\circ$	180 ~ 360	e_2	1 ~ 20	$k_0/(\text{N}/\text{mm})$	1 ~ 20

Table IV. The optimized parameters of exoskeleton.

Design variable	Taking values	Design variable	Taking values	Design variable	Taking values
l_{AB}/mm	30.002	$\theta_D/^\circ$	262.575	a	-3.524
l_{CD}/mm	79.463	$\theta_0/^\circ$	-28.222	b	13.463
l_{EF}/mm	20.027	x_{01}/mm	73.125	c	7.199
$\theta_A/^\circ$	44.388	y_{01}/mm	59.687	d	9.473
$\theta_B/^\circ$	0.054	e_1	14.64	e	4.753
$\theta_C/^\circ$	182.73	e_2	1.132	$k_0/(\text{N}/\text{mm})$	5.234

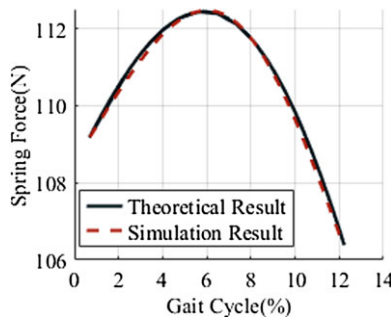


Figure 19. Comparison of human-machine instantaneous center trajectory.

(3) Constraint condition

The movement of the exoskeleton is mainly realized by an eight-bar mechanism. The composition and motion conditions of the eight-bar mechanism are expressed as

$$\begin{cases} 10 \leq \theta_1 - \theta_2 \leq 80 \\ 10 \leq \theta_3 - \theta_4 \leq 80 \end{cases} \quad (39)$$

The exoskeleton size parameters are constrained according to the Chinese adult human body size parameters, and the exoskeleton spring stiffness is selected according to the knee joint torque [26, 27]. The exoskeleton parameter constraints are shown in Table III.

The GA toolbox in the MATLAB software optimization toolbox is used to optimize the size parameters and spring stiffness of the exoskeleton. The optimized exoskeleton size parameters and spring stiffness are shown in Table IV.

According to the optimization results, the instantaneous center trajectory and joint torque of the exoskeleton are calculated and compared with the knee joint. Human-machine instantaneous center trajectory and joint torque are shown in Figs. 19 and 20, respectively.

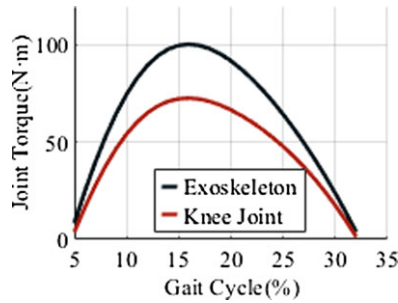


Figure 20. Comparison of exoskeleton joint torque and knee joint torque.

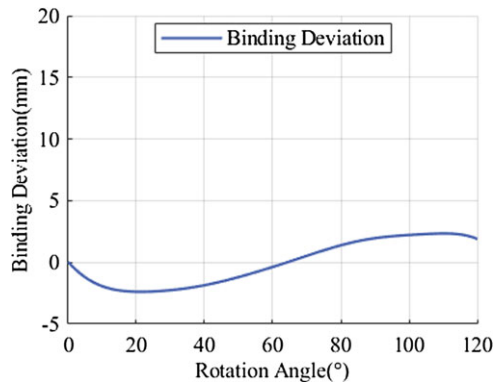


Figure 21. The deviation degree of human-machine binding.

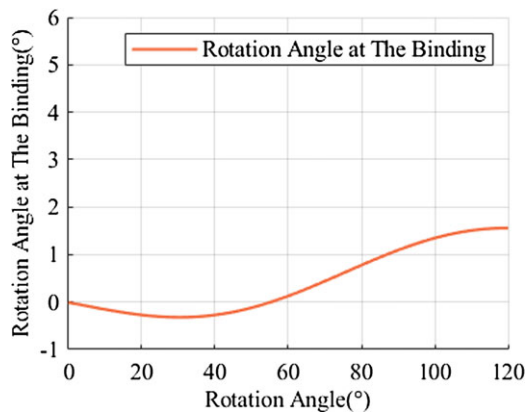


Figure 22. Rotation angle of human-machine binding.

From Figs. 19 and 20, it is evident that the optimized exoskeleton is designed to precisely follow the movement of the human knee joint during use. The joint torque of the optimized exoskeleton also matches the trend of human knee joint torque. However, the actual power torque of the exoskeleton should be greater than the knee joint torque.

Based on the results of the optimization, the deviation and rotation angle of the human-machine binding can be evaluated and visualized, as shown in Figs. 21 and 22, respectively.

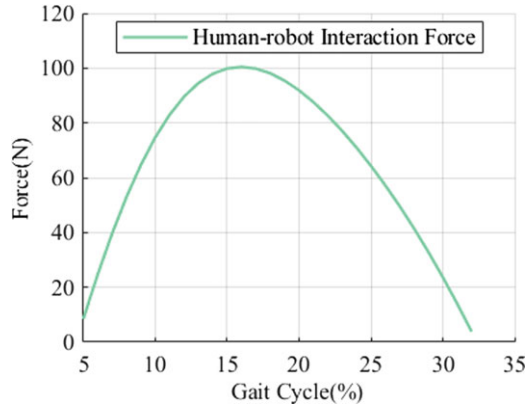


Figure 23. Human-machine interaction force at the binding.

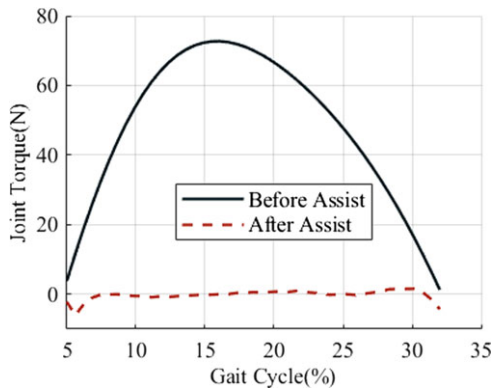


Figure 24. Knee joint torque after assist.

From Figs. 19, 21, and 22, it is evident that the optimized exoskeleton exhibits reduced strain on the knee joint and effectively aligns with the natural movement of the knee joint. Consequently, the optimized exoskeleton demonstrates superior characteristics in terms of human-machine interaction.

According to the exoskeleton joint torque shown in Fig. 20, the human-machine interaction force and knee joint dynamics at the binding are obtained, as shown in Figs. 23 and 24, respectively.

By comparing Figs. 24 and 20, it is evident that despite the optimized exoskeleton joint torque surpassing the knee joint torque, the knee joint torque experiences a substantial reduction due to the influence of human-machine interaction force. This observation implies that the exoskeleton effectively provides assistance to the human knee joint.

5.2. Kinematic and dynamic simulation analysis of exoskeleton

The three-dimensional model of the knee joint exoskeleton is established in SolidWorks software, and the structural parameters are set. Then the model is imported into ADAMS to construct a dynamic simulation model for simulation analysis, as shown in Fig. 25.

In order to estimate the instantaneous motion trajectory of the exoskeleton since it cannot be directly obtained, the motion of the slider in the virtual prototype is used as a substituted in Eqs. (3) and (14). This allows us to calculate the instantaneous position of the exoskeleton and compare it with the theoretical trajectory. The results are shown in Fig. 26. Moreover, the exoskeleton joint torque is analyzed

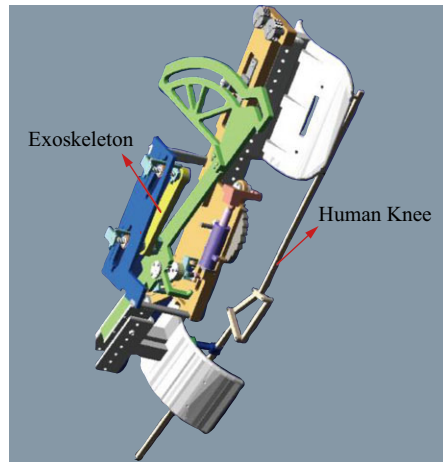


Figure 25. The exoskeleton model imported into ADAMS.

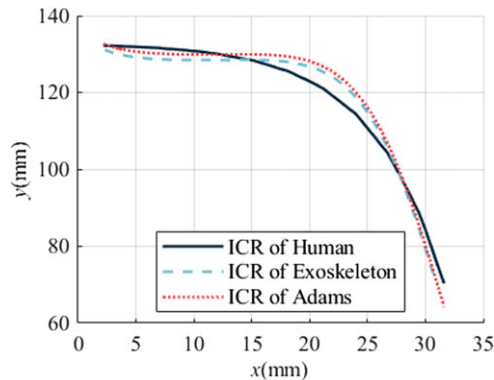


Figure 26. Comparison of instantaneous center trajectory.

by comparing the changes in spring elasticity, and the spring elasticity comparison results are shown in Fig. 27.

The comparison between Figs. 26 and 27 reveals that the instantaneous center trajectory and the changes in spring elastic of the exoskeleton align closely with the theoretical results. This consistency indicates that the optimized exoskeleton size parameters and spring stiffness are accurate and reliable.

5.3. Biomechanical simulation analysis based on OpenSim

The human model provided in OpenSim database is selected, and combined with the situation after exoskeleton is worn, the human-machine interaction model after exoskeleton is built, as shown in Fig. 28.

Using OpenSim simulation, the knee joint torque is evaluated before and after the exoskeleton is worn, as shown in Fig. 29. According to the research [28], the main force stage of the knee joint during human walking is when the muscle is performing positive work, resulting in positive joint torque. Subsequent to wearing the exoskeleton, the maximum forward joint torque experienced by the human body is markedly decreased, while the joint torque experienced during other stages does not exhibit significant increases. These findings indicate that the exoskeleton has a valuable assistive effect. The exoskeleton is found to

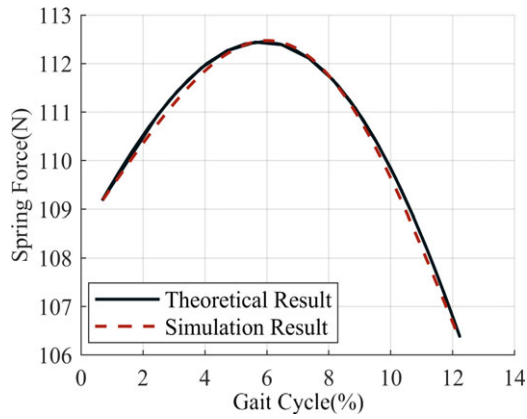


Figure 27. Comparison of spring elasticity.

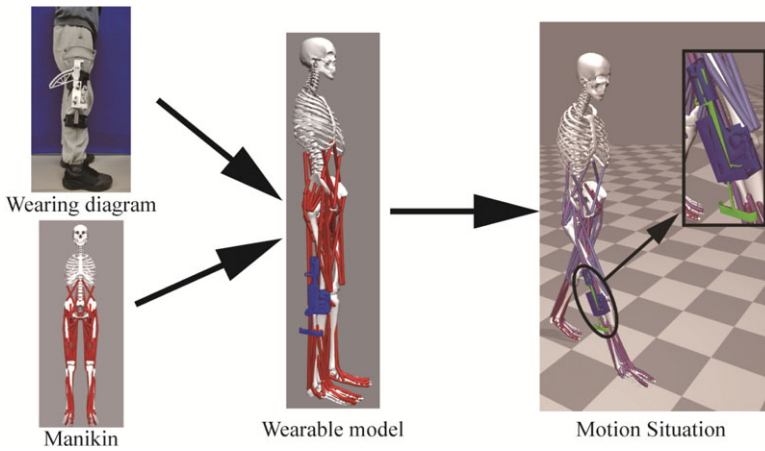


Figure 28. The simulation model is established according to the wearing condition of the exoskeleton.

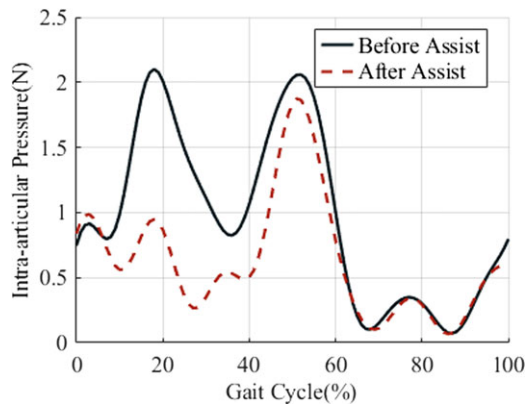


Figure 29. Knee joint torque before and after wearing exoskeleton.

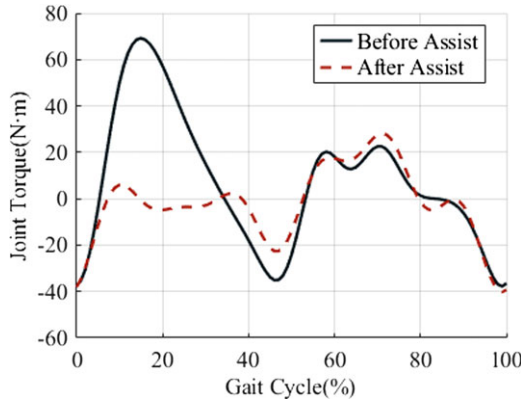


Figure 30. Knee joint pressure before and after wearing exoskeleton.

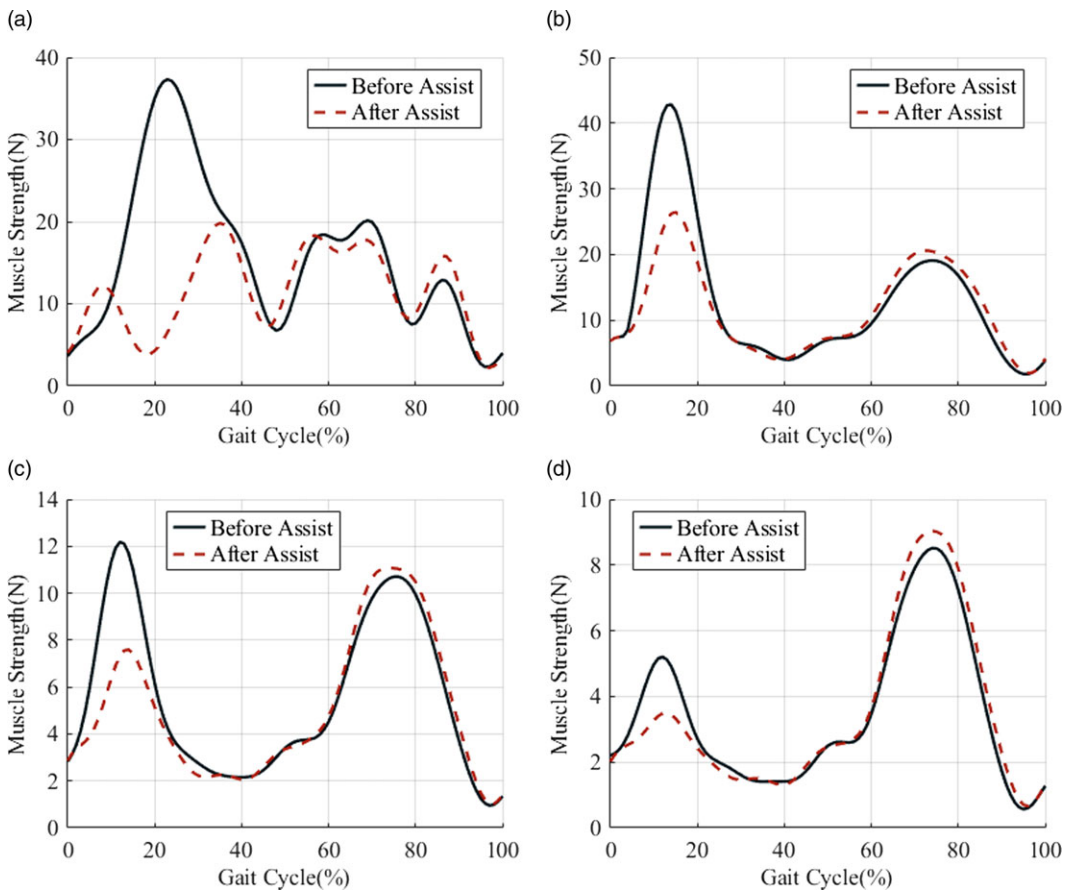


Figure 31. The strength of each muscle. (a) Rectus femoris muscle strength before and after wearing exoskeleton. (b) Lateral femoral muscle strength before and after wearing exoskeleton. (c) Medial femoral muscle strength before and after wearing exoskeleton. (d) Middle femoral muscle strength before and after wearing exoskeleton.

have reduced the human knee joint torque by a total of 48.42%. The pressure changes occurring within the knee joint during exercise are shown in Fig. 30.

During walking, the positive torque generated by the knee joint is mainly generated by the extensor muscles of the knee joint. The extensor muscles of the knee joint are mainly composed of the rectus, medialis, lateralis, and medialis muscles. To further verify whether the exoskeleton has an auxiliary effect on the extensor muscle group, we analyzed the torque variation of each muscle in the extensor muscle group. The strength of rectus femoris, lateral femoris, medial femoris, and middle femoral before and after wearing the exoskeleton are shown in Fig. 31(a), (b), (c), and (d) respectively.

After calculation, the muscle strength of rectus femoris, vastus lateralis, vastus medialis, and vastus intermedius decreased by 26.89%, 11.55%, 7.51% and 0.31%, respectively, after wearing exoskeleton. The exoskeleton mainly assists the knee joint during the load-bearing reaction period and the middle stage of the support phase, reducing the positive torque that causes the knee joint to extend during this stage. According to the relevant medical literature, the rectus femoris, vastus lateralis, and vastus medialis jointly provide the power to produce positive torque, so the strength of the three decreases significantly, while the vastus medialis plays a role in fastening the three muscles, so the decline is very small. By analyzing the force of each muscle that produces the knee joint extension torque, it is further proved that the exoskeleton has the performance of assisting the knee joint.

6. Conclusions

In this paper, a new exoskeleton configuration for assisting knee joint movement was proposed. The exoskeleton can assist knee joint movement while satisfying knee joint movement and reduce knee joint force and intra-articular pressure during movement. At the same time, the kinematic model and dynamic model after wearing the exoskeleton were established, and the deviation of human-machine binding during the movement and the effect of the exoskeleton on the knee joint were obtained. Then, according to the human-machine kinematic model and dynamic model, the size parameters and spring stiffness of the exoskeleton were optimized. The optimized exoskeleton human body model was simulated.

The final simulation results show that the exoskeleton has a certain assist effect, which can reduce the torque and intra-articular pressure of the knee joint during walking. After that, the exoskeleton will be tested to verify the assist effect of the exoskeleton and the feasibility of the overall mechanism scheme.

Author contributions. Jun Wei and Shizhao Zhang wrote the paper, and Jun Wei and Jianjun Zhang designed the study.

Financial support. This work was supported by the National Natural Science Foundation of China 52075145, the Hebei Province Natural Science Foundation Project E2022202130, the Major Scientific and Technological Achievements Transformation Project in Hebei Province 20281805Z, and the Central Government guides basic research projects of Local Science and Technology Development Funds Grant Number 206Z1801G.

Competing interests. The authors declare no competing interests.

Ethical approval. None.

References

- [1] J. S. Preston, D. Kbateman and A. J. Triajr, "Constraint in revision total knee arthroplasty," *Master. Ortho. Tech. Rev. Knee Arth.* **1**(3), 1–7 (2019).
- [2] J. S. Lora-Millan, F. J.é Sanchez-Cuesta, J. P. Romero, J. C. Moreno and E. Rocon, "A unilateral robotic knee exoskeleton to assess the role of natural gait assistance in hemiparetic patients," *J. Neuroeng. Rehabil.* **19**(1), 109 (2022).
- [3] A. J. Young and D. P. Ferris, "State of the art and future directions for robotic lower limb exoskeletons," *IEEE Trans. Neur. Sys. Reh. Eng.* **25**(2), 171–182 (2017).
- [4] S. Gregory, N. Owen, K. Inseung and J. Aaron, "The exoskeleton expansion: Improving walking and running economy," *J. Neuro Eng. Rehab.* **17**(3), 17–25 (2020).

[5] M. P. de Looze, T. Bosch, F. Krause, K. S. Stadler and L. W. O’Sullivan, “Exoskeletons for industrial application and their potential effects on physical work load,” *Ergonomics* **59**(5), 671–681 (2016).

[6] M. Gao, Z. Wang, S. Li, J. Li, Z. Pang, Z. Duan and H. Wang, “Design of Knee Exoskeleton Robot Based on Human Physiology,” **In: IEEE International Conference on Real-time Computing and Robotics (RCAR)** (IEEE, 2022) pp. 579–583.

[7] Y. Han, S. Zhu, Z. Zhou, Y. Shi and D. Hao, “Research on a multimodal actuator-oriented power-assisted knee exoskeleton,” *Robotica* **35**(9), 1906–1922 (2017).

[8] B. Chen, J. Tan, C. Shi and B. Zi, “Development of knee exoskeleton for capturing energy from human knee motion,” *Robotica* **41**(10), 3195–3210 (2023).

[9] S. D. Masouros, A. M. J. Bull and A. A. Amis, “Biomechanics of the knee joint,” *Ortho. Trauma* **24**(2), 84–91 (2010).

[10] A. Esquenazi, M. Talaty, A. Packel and M. Saulino, “The ReWalk powered exoskeleton to restore ambulatory function to individuals with thoracic-level motor-complete spinal cord injury,” *J. Phys. Med. Rehab.* **91**(11), 911–921 (2012).

[11] M. Talaty, A. Esquenazi and J. E. Briceno, “Differentiating Ability in Users of the ReWalk (TM) Powered Exoskeleton: An Analysis of Walking Kinematics,” **In: IEEE International Conference on Rehabilitation Robotics** (IEEE, 2013) pp. 1–5.

[12] D. Wang, K.-M. Lee and J. Ji, “A passive gait-based weight-support lower extremity exoskeleton with compliant joints,” *IEEE Trans. Robot.* **32**(4), 933–942 (2016).

[13] W. Yang, C. Yang and Q. Wei, “Design of an Anthropomorphic Lower Extremity Exoskeleton with Compatible Joints. **In: 2014 IEEE International Conference on Robotics and Biomimetics (ROBIO)** (2014) pp. 1374–1379.

[14] J.-H. Kim, M. Shim, D. H. Ahn, B. J. Son, S.-Y. Kim, D. Y. Kim, Y. S. Baek and B.-K. Cho, “Design of a knee exoskeleton using foot pressure and knee torque sensors,” *Int. J. Adv. Robot. Syst.* **12**(8), 112–112 (2015).

[15] K. J. Kim, M. S. Kang, Y. Choi, H. Y. Jang, J. Han and C. Han, “Development of the exoskeleton knee rehabilitation robot using the linear actuator,” *Int. J. Precis. Eng. Manuf.* **13**(10), 1889–1895 (2012).

[16] H. J. Kim, D. H. Lim and C. S. Han, “Development of a passive knee mechanism for lower extremity exoskeleton robot,” *J. Korea Robot. Soc.* **12**(2), 107–115 (2015).

[17] M. Olinski, A. Gronowicz and M. Ceccarelli, “Development and characterisation of a controllable adjustable knee joint mechanism,” *Mech. Mach. Theory* **155**, 104101 (2021).

[18] H. Lee, E. J. Rouse and H. I. Krebs, “Summary of human ankle mechanical impedance during walking,” *IEEE J. Trans. Eng. Health Med.* **4**, 2100407 (2016).

[19] R. Riener, M. Rabuffetti and C. Frigo, “Stair ascent and descent at different inclinations,” *Gait Posture* **15**(1), 32–44 (2002).

[20] D. Wang, K.-M. Lee and J. Ji, “A passive gait-based weight-support lower extremity exoskeleton with compliant joints,” *IEEE Trans. Robot.* **32**(4), 933–942 (2002).

[21] K. M. Lee and D. H. Wang, “Design Analysis of a Passive Weight-Support Lower-Extremity-Exoskeleton with Compliant Knee-Joint,” **In: IEEE International Conference on Robotics and Automation** (IEEE, 2015) pp. 5572–5577.

[22] B. Li, B. Yuan, S. Tang, Y. Mao, D. Zhang, C. Huang and B. Tan, “Biomechanical design analysis and experiments evaluation of a passive knee-assisting exoskeleton for weight-climbing,” *Ind. Robot.* **45**(4), 436–445 (2018).

[23] P. S. Walker, H. Kurosawa, J. S. Rovick and R. A. Zimmerman, “External knee joint design based on normal motion,” *J. Rehab. Res. Devel.* **22**(1), 9–22 (1985).

[24] G. Chen, Y. Xu, C. Yang, X. Yang, H. Hu, X. Chai and D. Wang, “Design and control of a novel bionic mantis shrimp robot,” *IEEE/ASME Trans. Mechatr.* **28**(6), 3376–3385 (2023).

[25] G. Chen, W. Peng, Z. Wang, J. Tu, H. Hu, D. Wang, H. Cheng and L. Zhu, “Modeling of swimming posture dynamics for a beaver-like robot,” *Ocean Eng.* **279**, 114550 (2023).

[26] State Bureau of Technical Supervision, “GB 10000-1988 human body dimensions of Chinese adults,” (Standards Press of China, Beijing, 1989).

[27] S. Y. Jiang. *Gait Analysis: Normal and Pathological Function*. 1st edition (Shanghai Science and Technology Press, Shanghai, 2017) pp. 67–72.

[28] Q. Guo, S. Li and D. J. Jiang, “A lower extremity exoskeleton: Human-machine coupled modeling, robust control design, simulation, and overload-carrying experiment,” *Math. Probl. Eng.* **16**, 1–15 (2015).

Appendix A

$$N_{11} = (e_1^2 + 2 \cos(2\theta_1 - 2\theta_2)e_2 + 1)$$

$$N_{12} = (-30 \cos \theta_2 - 234 \sin \theta_2)e_1^2 + (-3\sqrt{1546} \cos(2\theta_1 - 3\theta_2 + 1.443)$$

$$- 6\sqrt{1546} \cos(\theta_2 - 2\theta_1 + 1.443) - 3\sqrt{1546} \cos(\theta_2 - 1.443))e_1$$

$$- (-\sin \theta_1 \cos \theta_1)(234 \cos \theta_2 + 30 \sin \theta_2) + \cos^2 \theta_1(234 \sin \theta_2 - 30 \cos \theta_2) + 60 \cos^4 \theta_1 \cos^3 \theta_2)$$

$$N_{13} = (1755 \sin 2\theta_2 - 13464 \cos^2 \theta_2 + 13689)e_1^2 + (6957 \cos(2\theta_1 - 2\theta_2) + 1755(\sin 2\theta_1 - \sin 2\theta_2) - 6732(\cos 2\theta_2 - \cos 2\theta_1))e_1 - [(6957(1 + \cos(2\theta_1 - 2\theta_2) - \cos(2\theta_1 + 0.255)))/2 - (6957(\cos(2\theta_2 + 0.255) + \cos(4\theta_1 - 2\theta_2 + 0.255)))/4]$$

$$N_{21} = -e_1 + 1$$

$$N_{22} = (15 \cos \theta_2 + 117 \sin \theta_2)e_1 + 3 \cos(\theta_1 - \theta_2)(5 \cos \theta_1 + 39 \sin \theta_1)$$

$$N_{31} = 2 \cos(\theta_1 - \theta_2)$$

$$M_{11} = (e_2^2 \sin \sigma_1 + (\sin \sigma_1 + \sin \sigma_2)e_2 + \sin \sigma_2)^2 e_1^2 - [(2e_2^2 \sin 2\sigma_3 + 2(\sin 2\sigma_4 + \sin 2\sigma_3)e_2 + 2 \sin 2\sigma_4)(e_2^2 \sin \sigma_5 + (\sin 2\sigma_6 + \sin 2\sigma_3)e_2 + \sin 2\sigma_6)e_1^2]/2$$

$$M_{12} = (2e_2^2 \sin 2\sigma_3 + 2(\sin 2\sigma_4 + \sin 2\sigma_3)e_2 + 2 \sin 2\sigma_4)(w_1 e_2^2 + w_2 e_2 + w_3)(e_1^2 + e_1) - (2e_2^2 \sin 2\sigma_1 + 2(\sin 2\sigma_1 + \sin 2\sigma_2)e_2 + 2 \sin 2\sigma_2)(p_1 e_2^2 + p_2 e_2 + p_3)(e_1^2 + e_1)e_1$$

$$M_{13} = (p_1 e_2^2 + p_2 e_2 + p_3)^2 (e_1 + 1)^2 - (2e_2^2 \sin 2\sigma_3 + 2(\sin 2\sigma_4 + \sin 2\sigma_3)e_2 + 2 \sin 2\sigma_3)(w_{c1} e_2^2 + w_{c2} e_2 + w_{c3})(e_1 + 1)^2$$

$$M_{21} = -e_2^2 \sin \sigma_1 - (\sin \sigma_2 + \sin \sigma_1)e_2 - \sin \sigma_2$$

$$M_{22} = (p_1 e_2^2 + p_2 e_2 + p_3)e_1 + (w_1 e_2^2 + w_2 e_2 + w_3)$$

$$M_{31} = e_2^2 \sin 2\sigma_3 + (\sin 2\sigma_4 + \sin 2\sigma_3)e_2 + \sin 2\sigma_4$$

$$w_1 = [(117 + y_{01}) \cos \sigma_8 + (15 + x_{01}) \sin(\sigma_8) + (y_{01} - 117) \cos \theta_2 + (15 - x_{01}) \sin \theta_2]/2 + l_{23} \cos(\theta - \sigma_8)$$

$$w_2 = [(117 + y_{01})(\cos \sigma_7 + \cos \sigma_8) + (15 + x_{01})(\sin \sigma_7 + \sin \sigma_8) + (y_{01} - 117)(\cos \theta_2 + \cos \sigma_9 + \cos \sigma_{10}) + (15 - x_{01})(\sin \theta_2 + \sin \sigma_9 + \sin \sigma_{10})]/2 + l_{EF}(\cos \sigma_9 + \cos \sigma_{10})$$

$$w_3 = [(117 + y_{01}) \cos \sigma_7 + (15 + x_{01}) \sin \sigma_7 + (y_{01} - 117) \cos \theta_2 + (15 - x_{01}) \sin \theta_2]/2 + l_{EF} \cos(\theta + \theta_0 - \sigma_7)$$

$$p_1 = [(117 + y_{01}) \cos \sigma_{12} + (15 + x_{01}) \sin \sigma_{12} + (y_{01} - 117) \cos \theta_2 + (15 - x_{01}) \sin \theta_2]/2 + l_{EF} \cos(\theta + \theta_0 - \sigma_{12})$$

$$p_2 = [(117 + y_{01})(\cos \sigma_{11} + \cos \sigma_{12}) + (15 + x_{01})(\sin \sigma_{11} + \sin \sigma_{12}) + (y_{01} - 117)(\cos \theta_2 + \cos \sigma_{13}) + \cos \sigma_{14} + (15 - x_{01})(\sin \theta_2 + \sin \sigma_{13} + \sin \sigma_{14})]/2 + l_{EF}(\cos \sigma_{13} + \cos \sigma_{14})$$

$$p_3 = [(117 + y_{01}) \cos \sigma_{11} + (15 + x_{01}) \sin \sigma_{11} + (y_{01} - 117) \cos \theta_2 + (15 - x_{01}) \sin \theta_2]/2 + l_{EF} \cos(\theta + \theta_0 - \sigma_{11})$$

$$w_{c1} = [l_{EF}^2 \sin 2\sigma_{18} + ((15 + x_{01}) \cos \sigma_{15} + (117 + y_{01}) \sin \sigma_{15} + (15 - x_{01}) \cos(\theta + \theta_0) + (y_{01} - 117) \sin t)l_{EF} + 15(y_{01} + y_{01} \cos 2\theta_4 - x_{01} \sin 2\theta_4) + 117(x_{01} \cos 2\theta_4 - x_{01} + y_{01} \sin 2\theta_4)]/2$$

$$\begin{aligned}
 w_{c2} &= l_{EF}^2(\sin 2\sigma_{17} + \sin 2\sigma_{18})/2 \\
 &+ [(15 + x_{01})(\cos \sigma_{17} + \cos \sigma_{18} + \cos(\theta + \theta_0) + (\cos \sigma_{19} + \cos \sigma_{20})/2)]/2 \\
 &+ [(117 + y_{01})(\sin \sigma_{17} + \sin \sigma_{18} - \sin(\theta + \theta_0) - (\sin \sigma_{19} + \sin \sigma_{20})/2)]l_{EF} \\
 &+ 117x_{01}(-1 + \cos 2\theta_3 + \cos 2\theta_4) \\
 &+ 117y_{01}(\sin 2\theta_3 + \sin 2\theta_4) + 15y_{01}(1 + \cos 2\theta_3 + \cos 2\theta_4) - 15x_{01}(\sin 2\theta_3 + \sin 2\theta_4) \\
 w_{c3} &= [l_{EF}^2 \sin 2\sigma_{17} + ((15 + x_{01}) \cos \sigma_{16} + (117 + y_{01}) \sin(\sigma_{16}) + (15 - x_{01}) \cos(\theta + \theta_0) \\
 &+ (y_{01} - 117) \sin \theta)l_{EF} + 15(y_{01} + y_{01} \cos 2\theta_4 - x_{01} \sin 2\theta_4) \\
 &+ 117(x_{01} \cos 2\theta_4 - x_{01} + y_{01} \sin 2\theta_4)]/2
 \end{aligned}$$

where

$$\left\{ \begin{array}{l} \sigma_1 = \theta_1 + \theta_2 - 2\theta_4 \\ \sigma_2 = \theta_1 + \theta_2 - 2\theta_3 \\ \sigma_3 = \theta_1 - \theta_4 \\ \sigma_4 = \theta_1 - \theta_3 \\ \sigma_5 = \theta_2 - \theta_4 \\ \sigma_6 = \theta_2 - \theta_3 \\ \sigma_7 = \theta_2 - 2\theta_3 \\ \sigma_8 = \theta_2 - 2\theta_4 \\ \sigma_9 = \theta_2 - 2\theta_3 + 2\theta_4 \\ \sigma_{10} = \theta_2 + 2\theta_3 - 2\theta_4 \end{array} \right. \left\{ \begin{array}{l} \sigma_{11} = \theta_1 - 2\theta_3 \\ \sigma_{12} = \theta_1 - 2\theta_4 \\ \sigma_{13} = \theta_1 - 2\theta_3 + 2\theta_4 \\ \sigma_{14} = \theta_1 + 2\theta_3 - 2\theta_4 \\ \sigma_{15} = \theta + \theta_0 + 2\theta_4 \\ \sigma_{16} = \theta + \theta_0 + 2\theta_3 \\ \sigma_{17} = \theta + \theta_0 + \theta_3 \\ \sigma_{18} = \theta + \theta_0 + \theta_4 \\ \sigma_{19} = \theta + \theta_0 - 2\theta_3 + 2\theta_4 \\ \sigma_{20} = \theta + \theta_0 + 2\theta_3 - 2\theta_4 \end{array} \right.$$